particles

MDPI

Article

Electrostatic Simulations for the DUNE ND-GAr Field Cage

Christopher Hayes and Jon Urheim *

Department of Physics, Indiana University Bloomington, 727 E. 3rd Street, Bloomington, IN 47405, USA; hayesch@iu.edu
* Correspondence: urheim@indiana.edu

Abstract: ND-GAr is one of three detector systems in the design of the DUNE Near Detector complex, which will be located on the Fermilab campus, sixty meters underground and 570 m from the source of an intense neutrino beam. ND-GAr will consist of a cylindrical 10-bar gaseous Argon Time Projection Chamber (TPC) and a surrounding sampling electromagnetic calorimeter embedded within a superconducting solenoid, the cryostat and yoke for which together serve as the pressure vessel. While various options for the specific configuration of ND-GAr are being explored, essential design work for the detector has moved forward in recent months. This document describes basic mechanical, electrostatic, and gas flow design features of the ND-GAr TPC and presents results of electrostatic simulations of the interior of the pressure vessel for both single and dual-anode arrangements. Simulations are implemented with the Elmer finite-element software suite and related programs.

Keywords: Elmer; Gmsh; ParaView; element size factor; pressure vessel; magnet; neutrino; argon; ND-GAr detector; simulation; field cage electrode; voltage strip; insulation layer; time projection chamber; Barrel ECAL; end cap ecal; voltage profile; electric field profile

Citation: Hayes, C.; Urheim, J. Electrostatic Simulations for the ND-GAr Field Cage. *Particles* **2022**, *5*, 110–127. https://doi.org/10.3390/particles5020010

Academic Editors: Diego González-Díaz and Paul Colas

Received: 14 February 2022
Accepted: 31 March 2022
Published: 6 April 2022

1. Introduction

Unique among the elements of the DUNE Near Detector complex, ND-GAr is a low-mass magnetic spectrometer and electromagnetic calorimeter that can be moved to operating positions on and off the beam axis. This enables precision measurements of neutrino interactions on argon to control systematic errors in the study of neutrino oscillations based on observations in the liquid argon-based DUNE Far Detector modules. ND-GAr will also measure the momentum of muons exiting from the liquid argon-based ND-LAr detector located immediately upstream, thereby enhancing its capabilities. The requirements that ND-GAr is being designed to meet are described elsewhere [1,2].

As the core detector component of ND-GAr, a time projection chamber (TPC) with a cylindrical geometry and its axis oriented transverse to the beam direction is optimal from the standpoint of resolution, acceptance, and cost [1,2]. With this geometry, it is possible to capitalize on the experience with gas TPCs operating in colliding beam experiments. More specifically, the overall design for the ND-GAr TPC is traceable to the TPC constructed and operated for the ALICE experiment [3,4] at the Large Hadron Collider at CERN. This choice is motivated in part by the ALICE readout chambers' availability for use by DUNE, owing to recent upgrades to the ALICE TPC. However, the two TPCs will not be identical as the ALICE TPC is an annular device with an inner cylindrical wall, necessary to accommodate the beam pipe and inner detector elements. Moreover, the ND-GAr TPC will operate in a high-pressure environment, which will bring about a host of other design changes.

In this report, we explore some of the mechanical and electrostatic considerations affecting the design of the TPC field cage and the choice of materials. These considerations also couple to the design of the TPC gas systems; we report on initial studies of possible gas volume and flow configurations here as well.

1.1. Key Components of the ND-GAr Detector

A cross-sectional diagram illustrating the current ND-GAr detector design is shown in Figure 1. Particle detection is made possible by several independent sub-detectors. The centrally located TPC operates with an argon-based gas at 10 atm. The TPC is surrounded by both barrel and end cap electromagnetic calorimeters (ECAL) (shown in blue), and all detectors are enclosed in a pressure vessel providing the 10 atm environment. The pressure vessel is constructed with an external cryostat, which will house a set of six superconducting coils capable of maintaining a strong magnetic field (B = 0.5 T) in the interior of the pressure vessel. Finally, a partial return yoke made of low-carbon steel (shown in dark red) surrounds the detector.

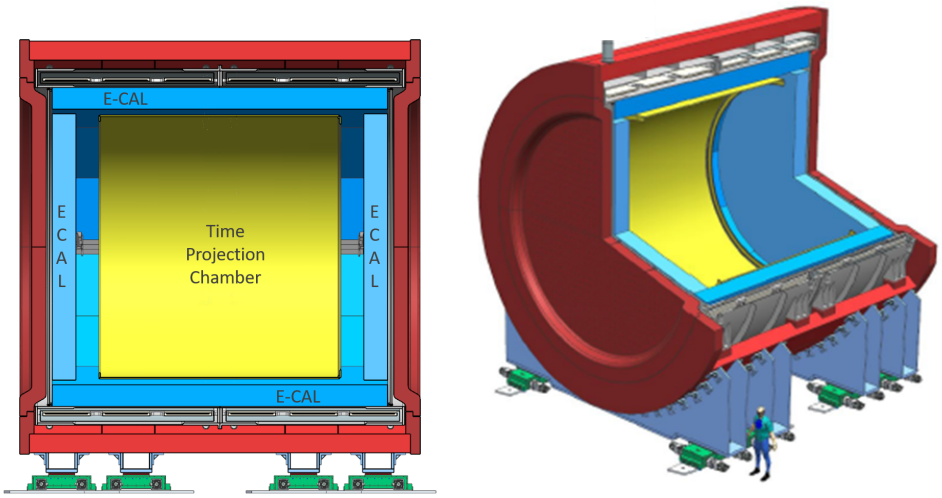

Figure 1. Cross-section of the ND-GAr detector and SPY magnet.

1.2. Pressure Vessel Gas Systems

The interior of the pressure vessel will contain at least three (possibly more) independent gas systems, and each gas system will be operated by a host of subsystems external to the pressure vessel. These subsystems are responsible for the purification, mixing, circulation, and monitoring of the gases in each volume. A general scheme for gas flow through the pressure vessel is illustrated in Figure 2. The drift volume gas for the interior of the TPC will have precisely monitored temperature and gas composition for tight controls on the electron drift velocity and diffusion properties of the medium. As both ends of the TPC will likely be fitted with readout chambers and other electronics, the flow of gas through the TPC will be transverse to the central axis of the device.

Any precise temperature requirement imposed on the drift volume may determine the temperature of the insulation layer gas volume, which would have no significant temperature requirements otherwise. The purpose of the insulation layer is two-fold: First, it must be designed so that no significant electric fields exist outside the TPC. This is important since the ECAL and other sub-systems exterior to the TPC will use sensitive electronics, which may be compromised by residual fields. Second, construction of the insulation layer must prevent the occurrence of a dielectric breakdown across the gap. This implies a minimum for the gap width and also imposes the requirement for a careful construction that is free from any sharp corners and which can produce locally large fields (See Section 3.6 for a discussion of Paschen's law and details on the determination of the gap width.).

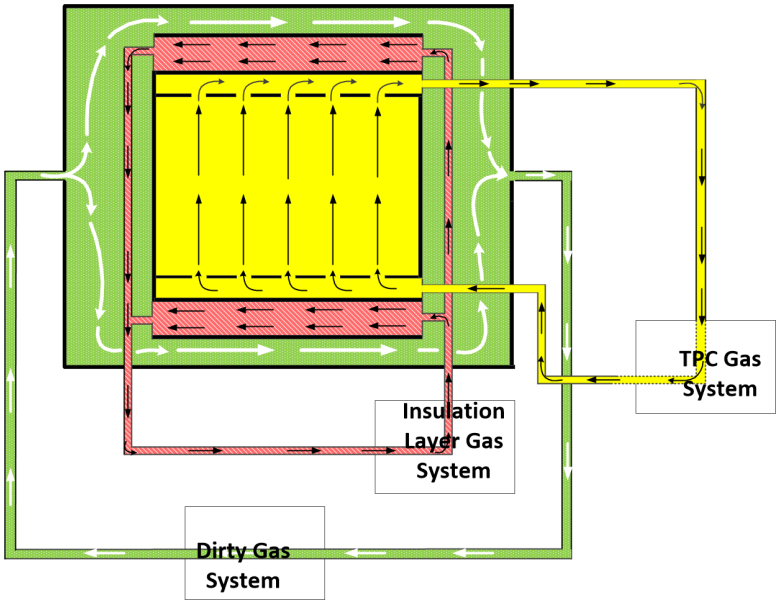

Figure 2. Gas systems for the ND-GAr pressure vessel for a dual-anode TPC.

The dirty (also ambient) gas volume is so named because it will likely receive out-gassed contaminants, mainly from polystyrene scintillator tiles that make up the ECAL, but also from other components external to the TPC. In addition, the function of the gas as a coolant may be important as both the ECAL and the TPC front-end electronics are heat-generating systems. Finally, it may be possible to combine the insulation layer with the ambient volume into a single gas system if it can be determined that out-gassed contaminants do not adversely affect the ability of the insulation layer to prevent a dielectric breakdown.

1.3. Single-Anode versus Dual-Anode TPC Design

The ALICE TPC design features a central cathode with two identical anodes for the detection of center-of-mass particle interactions from colliding beams. In contrast, the DUNE ND-GAr TPC will detect particles (roughly) perpendicular to the TPC central axis, thereby eliminating the requirement for the dual-anode design. Furthermore, recent discussions on the installation of a photon detection system generally favor a single-anode design. As such, the electrostatic simulations in this document are prepared for both design options (Figures 2–4 are prepared for a dual-anode device and would require modifications for single-anode designs.).

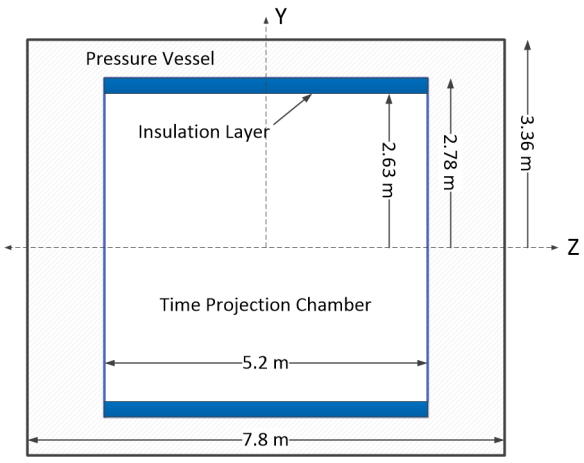

Figure 3. Dimensions of the field cage and pressure vessel.

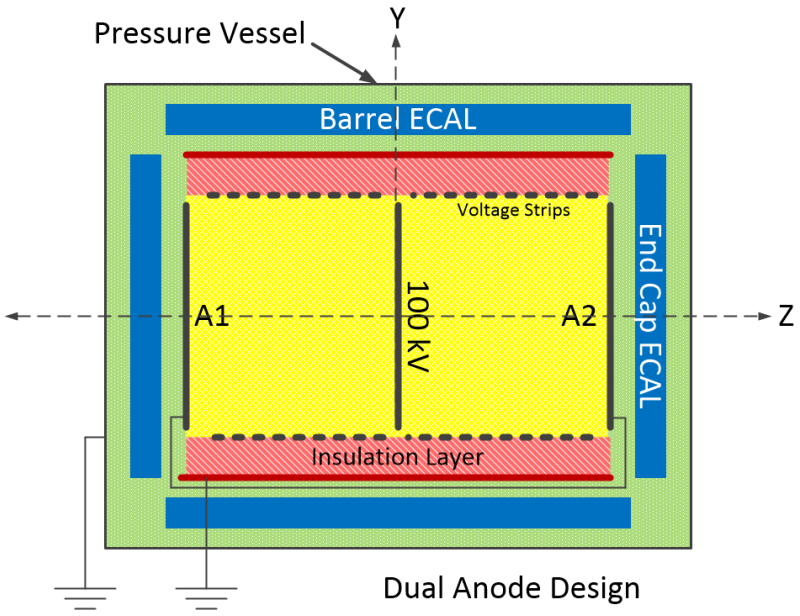

Figure 4. Placement of voltages in the dual-anode design.

2. Software for Electrostatic Simulations

The preparation of electrostatic simulations employs a suite of three open source software packages that feature an extensive user base. The Gmsh finite-element mesh-generating software [5] is used to develop the geometry in the interior of the pressure vessel. Once the geometry is specified, the Gmsh meshing tool is used to create a mesh of predetermined granularity throughout the volume. The associated mesh file may then be imported into the Elmer finite-element software suite [6–9], where the electrostatic problem is defined by specifying dielectric constants for materials in each sub-volume. Voltages can then be specified for all boundary conditions appropriate to the simulation. Final solutions generated from Elmer can be read by ParaView [10,11] or another visualization software tool (Color images of electric field profiles and voltage profiles in this document are all prepared exclusively with ParaView software. Plots of the voltage and components of the electric field vector are also generated by ParaView analysis tools.).

2.1. Source Information for Mesh Preparation

The construction of meshes for the development of the simulations rely on two sources of information. All dimensions for the TPC are chosen in accordance with known design parameters for the ALICE TPC, which are well-documented in the ALICE TDR and other related documents [3,4]. Dimensions of the Pressure vessel, the ECAL, and other parts of the ND-GAr detector are taken from the ND-GAr Magnetic Design document [12]. A simple diagram indicating the dimensions of the TPC and the pressure vessel used for the electrostatic simulations in this document is shown in Figure 3.

2.2. Mesh Granularity in Gmsh

An important criterion for the preparation of electrostatic simulations is the chosen value for mesh granularity. This is determined by specifying the *Element Size Factor* (ESF), which is essentially the distance between adjacent nodes on the mesh along any axis. This number can also be used to determine the total number of nodes used for a given geometry. From Figure 3 above, the total volume of the pressure vessel is $V = 277$ m^3. For an ESF of 5.0 cm, the total number of nodes is as follows:

$$\mathrm{N} = \mathrm{V}/(\mathrm{ESF})^3 \approx 2.2 \text{ million} \quad (1)$$

In general, the precision of the electrostatic simulations can be traced to the value of the ESF. No problems arise for simulations of voltage as these values are specified by the user on specific boundaries and then interpolated throughout the volume by the software. Instead, problems arise when the software calculates electrostatic fields, which may only be determined within the spatial resolution of the mesh nodes.

This effect can be mitigated by decreasing the value of the ESF for the geometry, but this will drive up the size of the $*$.msh file used to create the simulation. Ultimately, the problem of precision for the simulations reduces the capabilities of the computer system on which the simulations are made. For the work performed here, the smallest ESF values that yielded useful results on the IU cluster computer were in the vicinity of ESF = 2.5 cm.

3. Electrostatic Simulations

The highest priority for the electrostatic simulations is to study the case of highly uniform electric fields near the ALICE value of 400 V/cm in the interior of the TPC. As the field cage has a length of 5.2 m, 200 kV is placed on the cathode for the single-anode design, and 100 kV is placed on the cathode for the dual-anode design. Anodes for the ND-GAr TPC will be defined by eighteen azimuthal sectors of readout chambers. The inner and outer readout chambers (IROCs and OROCs) for each sector are those of the ALICE TPC, but ND-GAr is required to add additional readout chambers in the central portion of the anode. Regardless of how this is accomplished, the complexity of readout chambers—with their multi-wire grid design—is difficult to replicate in an electrostatic simulation with the capabilities of the software. For this reason, a monolithic anode with a voltage set to zero is considered for the simulation.

3.1. Gmsh Model for Electrostatic Simulations

The geometry of the interior of the pressure vessel is developed from a single Gmsh model with the capability of producing both single and dual-anode electrostatic simulations. The volumes defined for the Gmsh model include the following:

a. Time Projection Chamber
b. Insulation Layer
c. Barrel ECAL
d. End Cap ECAL
e. Space between volumes

Several diagrams produced directly from the Gmsh model are included in Figure A1 in Appendix A, illustrating their overall design and placement inside the pressure vessel boundary. For each volume, ElmerGUI requires the identification of a material. For the electrostatic problem, this translates into the specification of the dielectric constant of the material. As the majority of the volumes inside the pressure vessel are filled with gases at (or near) 10 atm, the dielectric constants are very close to vacuum and may be set to one [13]. This is not true for the volumes specified as barrel and end cap ECAL, for which large portions of the geometry are specified as layers of (mostly) polystyrene plastic and a metal such as lead, copper, or steel. In this case, the dielectric constant for polystyrene, with a value of $\varepsilon = 2.55$, is chosen for the entire volume.

3.2. Specification of Voltages

After all materials are appropriately specified, ElmerGUI requires the application of voltages onto all specified boundaries to solve the electrostatic problem. These boundaries are not individual volumes endowed with some non-zero thickness, and they do not require any identification with a material. Instead, cathode and anode planes are round surfaces having a radius equal to the inner radius of the TPC. Field cage electrodes (voltage strips) are modeled as short cylindrical surfaces located along the interior surface of the barrel part of the TPC vessel (see Figure 4). These strips have a width of 10 cm and are placed 2.5 cm apart. The approximation that the cathode and the voltage strips are surfaces without a thickness is not too far from a realistic model. In the ALICE design, the cathode is a

stretched mylar foil, aluminized on both sides, and having a thickness of 23 microns. The voltage strips are also aluminized mylar having a thickness of 25 microns. However, as noted earlier, the approximation does not apply to the anodes.

For the central dual-anode design, 100 kV is placed on the cathode, with 0 kV placed on each anode. A formula for voltages applied to the 21 strips on both sides of the central cathode is as follows:

$$V_2(n) = 4.5455 \cdot n \qquad 1 \leq n \leq 21 \qquad \text{units are kV} \tag{2}$$

For the single-anode design, the insulation layer is extended to cover the end cap of the TPC. A cathode voltage of $V = 200$ kV is applied to the "inside" of the end cap, with only 0 kV placed on the anode. Beginning from zero at the anode, voltages specified on the voltage strips must be set to increase incrementally over the entire length of the TPC. The corresponding voltage formula for the strips on the single-anode device is the following:

$$V_1(n) = 4.6512 \cdot n \qquad 1 \leq n \leq 42 \qquad \text{units are kV} \tag{3}$$

The number of voltage strips chosen here as well as their thickness are somewhat small compared to the ALICE TPC, which was fitted with over 300 voltage strips spanning its approximate five-meter length. However, the purpose here is to generate field and voltage profiles and illustrate the general behavior of the fields. Simulations using a larger number of strips is available in Section 3.5.

For both single and dual-anode designs, the exterior surface of the insulation layer is also set to ground. This is a cylindrical surface for the dual-anode design and a cup-shaped surface for the single-anode design. As the outer insulation layer is connected to the anodes, this effectively grounds an entire closed surface surrounding the TPC.

A separate ground is also anticipated for the closed surface defining the pressure vessel, as illustrated in Figure 4. It is sufficient to indicate that simulations performed with the extra ground show only minor changes to the original simulations. Even so, a ground applied to the pressure vessel wall is required to eliminate charge build-up and to control electronic noise—effects which are beyond the scope of results produced by the simulations.

3.3. Field Profiles

Illustrations of the electrostatic fields over a cross-section through the central axis of the pressure vessel are generated by ParaView for both designs and are available in Figures 5 and 6. The most important aspect of these illustrations is the highly uniform field in the interior of the TPC. In contrast, there are very large and variable fields shown in red, orange, and yellow, which exist in the insulation layer. Another key aspect of the figures is the absence of any sizeable electrostatic footprint outside of the TPCs and the insulation layers. Neither the barrel nor end cap ECAL could be seen by the simulations, implying that relatively insignificant fields exist in these regions.

For the dual-anode design, a thin dark-blue line at the center (possibly difficult to see) marks the central cathode at 100 kV. The inherent width of the central cathode is driven by the element size factor of 2.5 cm chosen for the simulation. It is a simple matter to calculate the largest field value in the insulation layer, which is accomplished by forming the ratio:

$$\mathrm{E}_{max} = \frac{\text{voltage applied to the cathode}}{\text{thickness of the insulation gap}} = \frac{100\mathrm{kV}}{0.147m} \approx 6.8 \times 10^5 \ \mathrm{V/m} \tag{4}$$

For the single-anode design, fields existing in the insulation layer—especially over the end cap—are a factor of two larger than those produced for the dual-anode design, reaching a maximum value in the vicinity of $\mathrm{E} = 1.3 \times 10^6$ V/m. The profile also features a sharp corner at the intersection of the end cap insulation layer and perimeter insulation layer, which causes an unduly large field. This issue could easily be eliminated by rounding the corner in the Gmsh model.

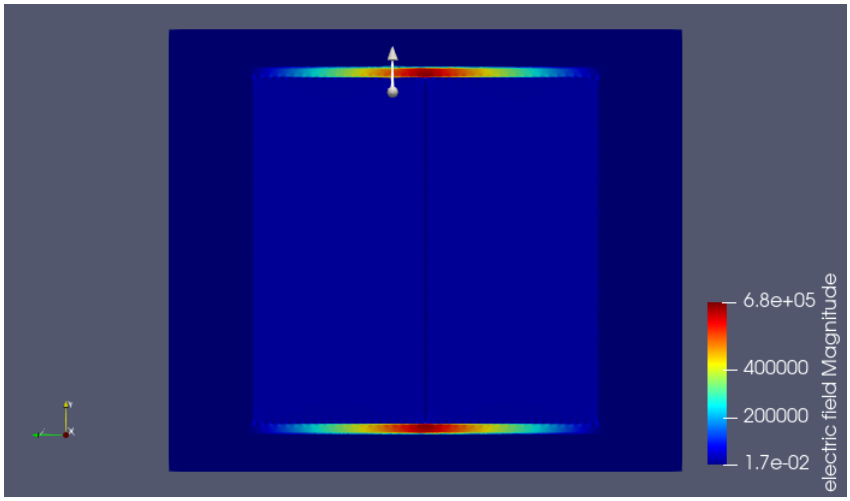

Figure 5. Electric field profile inside the pressure vessel for the dual-anode design.

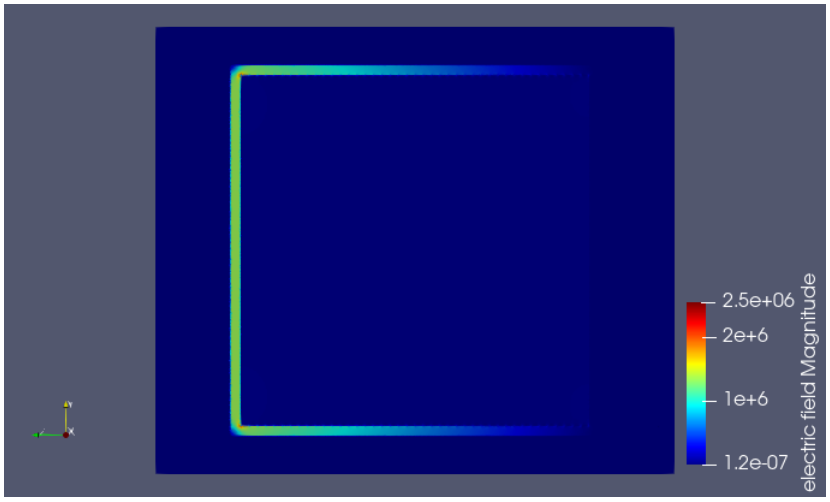

Figure 6. Electric field profile inside the pressure vessel for the single-anode design.

In addition to the field profiles already given, voltage profiles generated by ParaView are also available in Figure 7. Although their usefulness as an analytical tool is limited, they clearly show that non-zero voltages only exist inside the TPC for both designs.

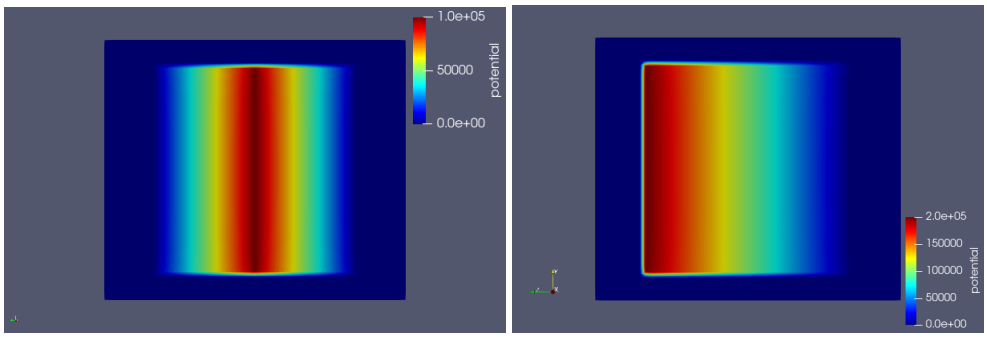

Figure 7. (**Left**): Voltage profile for the dual-anode design. (**Right**): Voltage profile for single-anode design.

Voltage and field plots drawn on the central axis of the TPC and across the insulation gap are also available in Appendices B and C.

3.4. Analysis of Fields in the TPC

While diagrams representing field and voltage profiles provide a good understanding of their behavior inside the pressure vessel, they do not adequately display small variations that exist within the TPC or their residual behavior in the region surrounding the TPC. For a more detailed assessment, it is useful to analyze the data generated by the simulations and made available with ParaView. Variations in the field component E_z in the interior of the TPC for the dual-anode design are illustrated in the top plot of Figure A4. Individual curves are plotted parallel to the symmetry axis of the cylinder at various distances, y, from the central z-axis. The plot is only drawn using data from one side of the TPC as a full-length plot would only show symmetry about the central cathode. The plots indicate the general trend for larger variations in E_z, with an increasing y. This trend is quantified in Table 1.

Table 1. Field variations in the TPC for the dual-anode design with 21 voltage strips per side.

Field E_z (V/m)	$y = 0.0$ **m**	$y = 1.0$ **m**	$y = 1.5$ **m**	$y = 2.0$ **m**	$y = 2.4$ **m**
Avg.	38,167	38,162	38,152	38,108	37,922
Max	38,256	38,355	38,594	39,439	43,034
Min	38,122	38,051	37,834	37,472	36,883
R_z = Max/Min	1.004	1.008	1.019	1.053	1.167

Even at y = 2.0 m from the central axis, values of R_z in the table indicate only small variations in E_z roughly at the 5% level. The value of y = 2.4 m in the last column of the table represents a sensible estimate of the radial boundary of the fiducial volume and is approximately equal to the largest radius covered by the readout chambers in the TPC design. Variations of E_z are more significant here, but precision in the field will obviously improve with the use of larger numbers of voltage strips. This issue is addressed in a methodical way in Section 3.5.

In addition to variations in the field component E_z, it is also prudent to perform a similar analysis on the transverse components E_x and E_y. Based on the cylindrical symmetry of design, an analysis of only one transverse component is necessary. We choose the component E_y, which is plotted parallel to the z-axis at different values of y in the bottom plot of Figure A4. With an average value of E_z already available from Table 1 at about 38,100 V/m, the largest deviation shown in the plots is only about 2% of the average value. This is still significant, however, and it is worthwhile to point out that the ALICE design specified maximum deviations of the electric field vector on the order of about 10^{-4}. While restrictions on field variations at this level are not expected for the ND-GAr TPC using an argon-based gas, the values quoted here may not be sufficient.

The analysis above is only performed for the dual-anode design, but a similar set of plots for the single-anode design is available in Figure A7. Further discussion of these plots is not warranted, but Table 2, which outlines similar characteristics for the single-anode design, has nevertheless been included.

Table 2. Field variations in the TPC for the single-anode design with 42 voltage strips.

Field E_z (V/m)	$y = 0.0$ **m**	$y = 1.0$ **m**	$y = 1.5$ **m**	$y = 2.0$ **m**	$y = 2.4$ **m**
Avg.	38,154	38,147	38,130	38,092	37,936
Max	38,514	38,676	38,981	39,833	42,241
Min	37,893	37,810	37,704	37,561	37,424
R_z = Max/Min	1.016	1.023	1.034	1.061	1.129

3.4.1. Fields near the Voltage Strips

The uniformity of the electrostatic field in the interior of the TPC is based on the number of voltage strips used for the simulation. Deviations from uniformity become apparent near the voltage strips, where the field profile inherits the repetitive structure of the strips. This is illustrated in Figure 8.

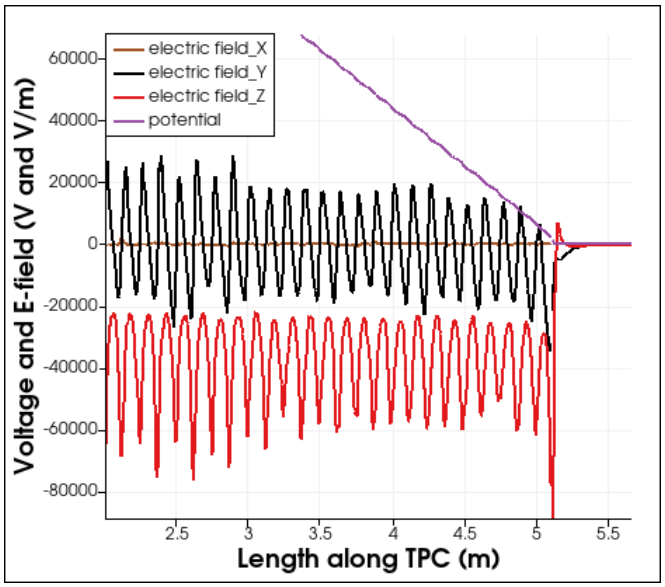

Figure 8. Oscillating non-uniformities in the y and z components of the electric field near the voltage strips.

In general, non-uniformities in the field can be mitigated using larger numbers of strips with smaller widths. However, since the precision of the fields produced by the simulation is related to the ESF chosen for the problem, strip widths smaller than the ESF value may not be useful.

3.4.2. Residual Fields outside the TPC

In addition to the analysis of the fields inside the TPC and the insulation layer, it is also important to discuss residual fields in the ambient gas volume, including fields inside the barrel and end cap ECAL (not shown in Figure 2). The only example of significant residual fields is illustrated by the plot in Figure 9, which shows the $\|E_z\|$ values from the edge of the pressure vessel up to the anode of the dual-anode TPC design.

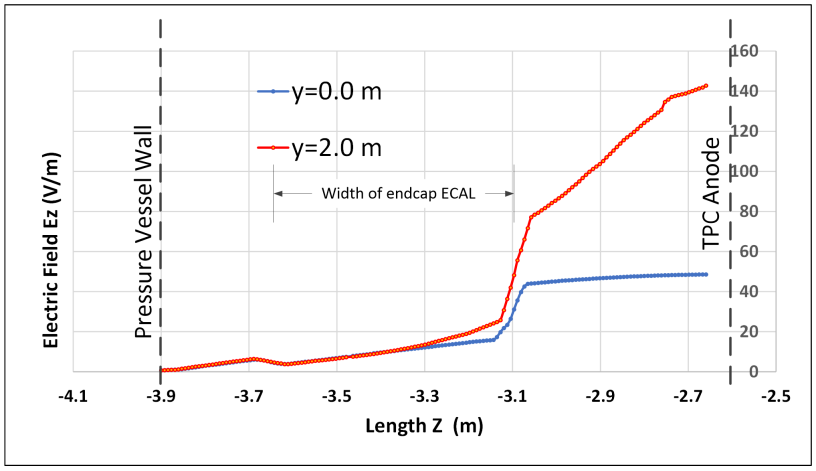

Figure 9. Blue: Electric field, E_z, outside the TPC on the central axis of the pressure vessel. Red: Same plot except displaced from the central axis by y = 2 m.

Residual fields are a symptom of the finite number of voltage strips, the pre-defined width of the strips, and the spacing between the strips. The value near 150 V/m adjacent to the anode is significant but is only about 0.3% of the nominal field inside the TPC. Both plots undergo a large dip in the region of -3.7 m < Z < -3.1 m, which can be attributed solely to the presence of the polystyrene in the hexagonal-shaped end cap ECAL located about 0.5 m away from either end of the TPC. Not shown in the plot are the residual values of the x and y components of the field in this region, which have values significantly smaller than the z component.

3.5. Optimized Electrostatic Field from Generic Simulations

A measure of the quality of a TPC is the uniformity of the electrostatic field in the drift volume. Clarity of particle tracks is easily lost when variations in individual field components alter the drift electron velocities and diffusion coefficients of the gas medium. Field uniformity has a strong dependence on the number of voltage strips surrounding the drift volume, and this may be quantified by the following definitions:

$$R_x \equiv \frac{E_x}{E_z} \qquad R_y \equiv \frac{E_y}{E_z} \qquad R_z \equiv \frac{E_z(max)}{E_z(min)} \tag{5}$$

Both R_x and R_y are simply ratios of the transverse components of the fields to the longitudinal components as determined by the simulation. In an ideal design, both of these ratios will vanish at all points inside the drift volume. The last ratio, R_z, has already appeared in Tables 1 and 2 and is a measure of the variation of the longitudinal field on any given line through the TPC parallel to the z-axis. For an ideal design, this ratio will always be 1.

The dependence of (R_x, R_y, R_z) on the number of voltage strips was determined by preparation of generic simulations for a single-anode TPC in the shape of a cylinder having a length of 5.0 m and a radius of 2.7 m. There were no volumes built into the Gmsh model external to the TPC, but the outer perimeter of the cylinder was set up by the Gmsh scripting language to accommodate variable numbers of voltage strips, with a constant strip spacing of 1 cm. Gmsh models using 6, 10, 15, 20, 50, and 100 voltage strips were imported into the ElmerGUI where voltages of 200 kV and 0 kV were applied to each end of the cylinder. Appropriately chosen incremental voltages were then applied to the strips, rendering six simulations.

Plots of $|E_z|$ along the central axis of each generic design showed a smooth curve, with a conspicuous peak at the center and symmetric between the cathode and the anode (similar to the plots in Figure A7). The left plot in Figure 10 shows values of R_z generated by the simulations and a simple formula fitting the curve.

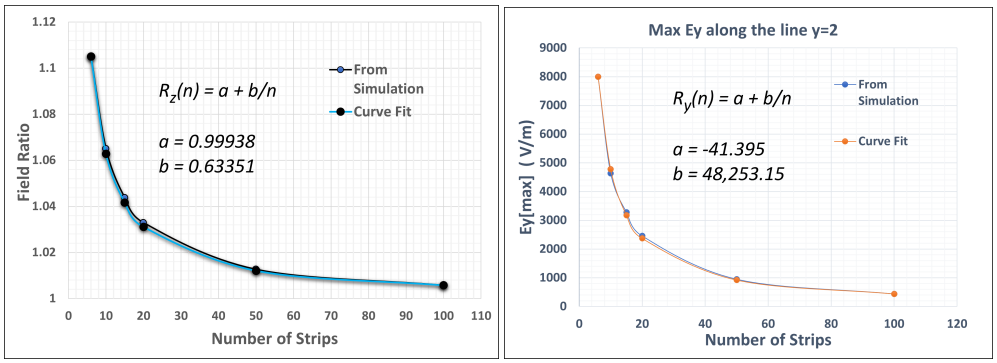

Figure 10. (**Left**): Uniformity of the field, E_z, on the central axis as a function of the number of voltage strips. (**Right**): Value of $R_y(max)$ measured at $y = 2$ m as a function of the number of voltage strips.

The curve itself is not surprising but has a usefulness in its ability to estimate the number of voltage strips based on requirements for maximal field variations. As an

example, if field variations in E_z are limited to 10^{-3}, then an extrapolation of the plot on a logarithmic scale suggests a number of field strips approaching 390. (For comparison, the ALICE TPC is designed with 330 voltage strips spaced over an approximate 5 m length. Strips are 1.5 cm wide and separated by 0.2 cm.)

Similar to the previous plot of R_z, the general trend for decreasing values of R_x and/or R_y with the number of voltage strips is illustrated on the right in Figure 10. The plot shows maximum values for R_y determined on the line $y = 2$ m, but it does not indicate the general trend that the maximums move slowly towards the cathode and the anode for larger values of n.

Removal of Residual Fields in the TPC

Even with large numbers of voltage strips specified for the TPC, residual fields in the interior of the drift volume may still exist based on the placement of the cathode and the anode relative to the strips. To understand the problem, simulations were prepared as in Figure 11, where all relevant parameters of the TPC, including the strip width, strip separation, and the number of strips, were kept constant, except for the ability to vary the positions of the cathode and the anode equally over small distances, z, next to closest voltage strip. The result of several simulations indicated that there exists an optimal position, z_o, which simultaneously eliminated all variations in the field component, E_z, over the length of the TPC as well as in the residual transverse fields E_x and E_y.

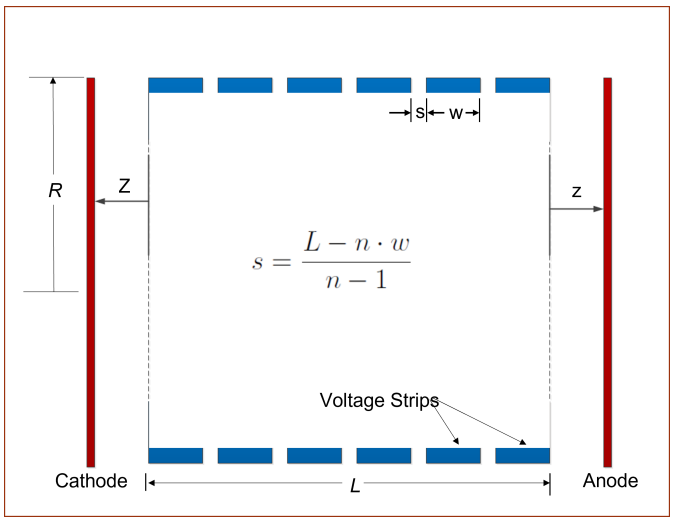

Figure 11. Model for the elimination of transverse fields and variations in the field E_z.

In other words, a good approximation for all points inside the drift volume can be calculated as follows:

$$(R_x, R_y, R_z) \longrightarrow (0, 0, 1) \tag{6}$$

Plots in Figure 12 show results for TPC simulations using 100 voltage strips, with $\Delta V = 100$ kV between the cathode and the anode. The plots indicate the disappearance of all residual fields when the cathode and anode were moved away from the voltage strips by a distance of 3.06 cm. At this distance, $R_z - 1$ was found to have a value of 3.9×10^{-5}.

It may be possible to calculate theoretical values for z_o from the first principles, given values of the strip widths w and strip spacing s. However, even if this can be accomplished, a real-world attempt to precisely place the cathode may be difficult to accomplish. Furthermore, the anode itself is typically composed of proportional wire chambers with a series of wire grids held at non-zero voltages. In order to get around this, a more reasonable equivalent plan would be to leave the distance z un-optimized and instead, tweak voltages on both electrodes to minimize the interior fields.

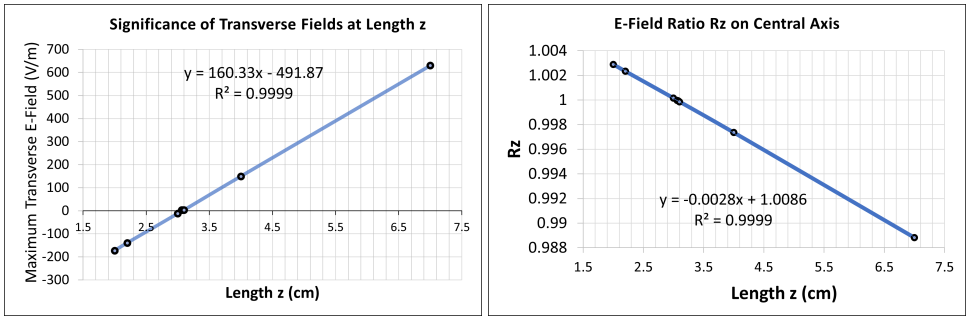

Figure 12. Plots showing the disappearance of residual fields in the TPC for a value of $z_o \sim 3.06$ cm. Simulated TPCs used 100 voltage strips, had an unperturbed length of 5 m, and used a strip width of 4 cm.

3.6. Field Cage Insulation Layer

Paschen's law determines the breakdown voltage between two electrodes immersed in a gas as a function of the gas pressure p and the separation d between the electrodes. This law may be applied directly to the insulation layer of the ND-GAr field cage. Most importantly, if the ALICE TPC gap length of 14.7 cm is maintained for the new design, the 10-atmosphere environment of the ND-Gar modifies the value of $p \cdot d$ to an order of magnitude larger than that of ALICE.

At present, a completed design plan specifying an appropriate gas that could flow through the insulation gap is not available. Nevertheless, research has been carried out by the University of Texas at Arlington (UTA) on the dielectric strength of candidate gases and gas mixtures [14]. This research suggests the notion of decreasing the gap width of the insulation layer to 6–10 cm for the ND-GAr detector. A design change such as this would have several notable advantages. Most notably, the effective diameter of the ND-GAr field cage would be smaller. In addition, the volume of gas used for the insulation layer would also be significantly reduced.

Data from UTA also suggest that breakdown voltages near 150 kV at 10 atmospheres may be achieved, which would work for the ND-GAr dual-anode design. However, large values of $p \cdot d$ are not available from the research. In addition, while Paschen's law is known to be valid for small values of $p \cdot d$, there is evidence that the law may become inaccurate for large values of $p \cdot d$, depending on the chosen gas. To compound the issue, experimental data at the high end of the Paschen curve are generally difficult to locate and will prompt an investigation of the ND-GAr detector to verify that specified voltages are well below the breakdown voltage.

4. Summary

Electrostatic simulations were prepared using the Elmer Finite-Element Software Suite, illustrating essential voltage and field profiles for the DUNE ND-GAr single/dual-anode TPC designs. Analysis of data showed in detail the behavior of the fields in the TPC, which led to further simulations that indicated how fields may be optimized by larger numbers of strips and also by the careful placement of the cathodes and anodes. Future investigations with newly developed techniques are needed for precision studies of tolerances on field variations. Future work will also benefit from more advanced stages of design, where the TPC gas mixture is uniquely identified and the choice of single/dual-anode arrangement is finalized.

Author Contributions: Conceptualization, C.H. and J.U.; methodology, C.H.; software, C.H.; validation, C.H. and J.U.; formal analysis, C.H.; investigation, C.H.; resources, C.H.; data curation, C.H.; writing—original draft preparation, C.H.; writing—review and editing, C.H.; visualization, C.H. and J.U.; supervision, J.U.; project administration, J.U.; funding acquisition, J.U. All authors have read and agreed to the published version of the manuscript.

Funding: This research was funded by the U.S. Department of Energy grant number DE-SC0010120.

Institutional Review Board Statement: Not applicable.

Informed Consent Statement: Not applicable.

Data Availability Statement: The data presented in this study are available on request from the corresponding authors.

Acknowledgments: We are grateful for the services of Nicholas Johnston whose expertise and programming skills on the IU Carbonate computer cluster was invaluable to the success of this research.

Conflicts of Interest: The authors declare no conflict of interest.

Appendix A. Images of the Gmsh Model

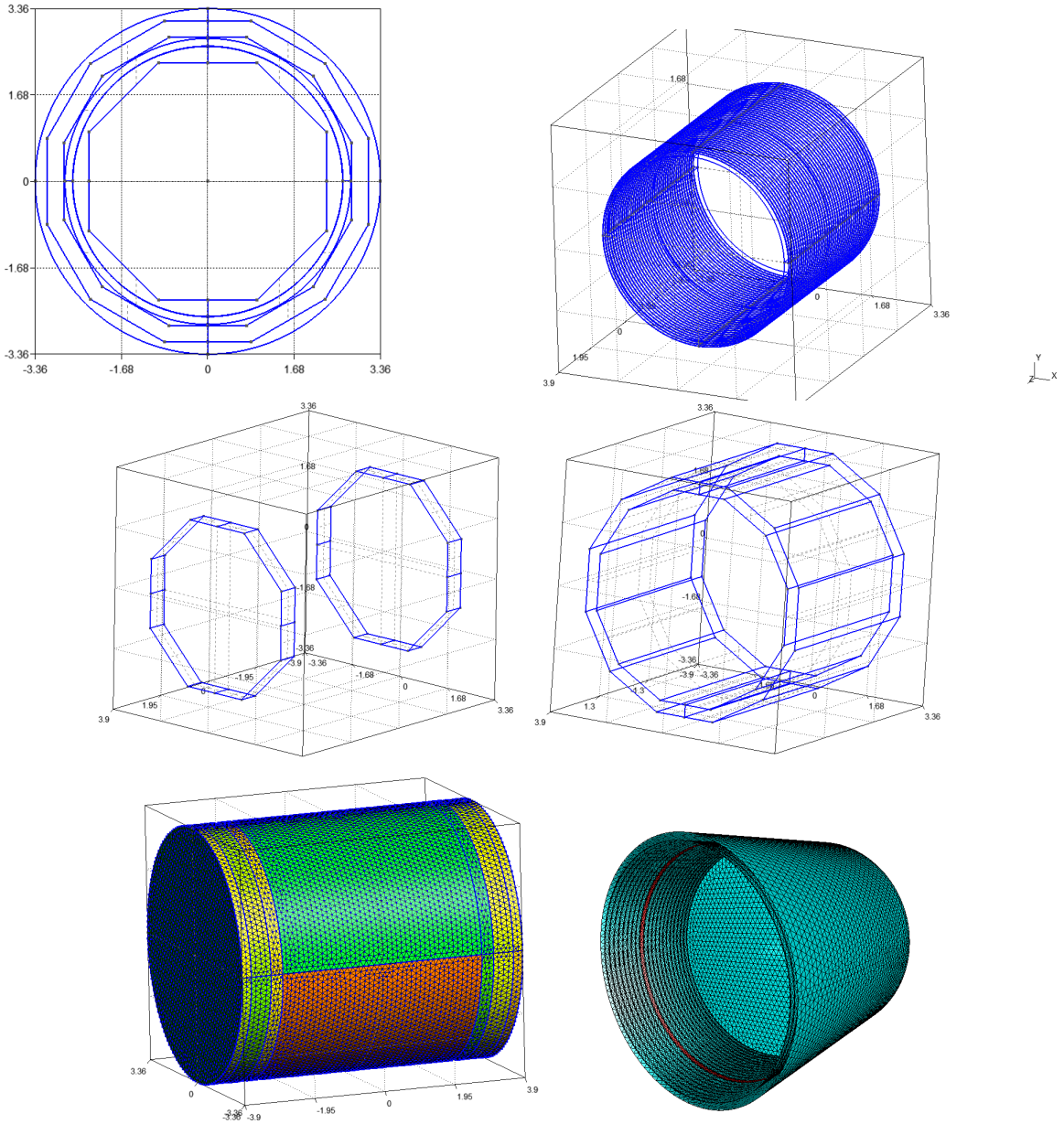

Figure A1. Images of the Gmsh model: (1) Cross section of entire geometry perpendicular to the z-axis. (2) Image of the TPC only with 10 cm wide voltage strips spaced by about 2.5 cm. (3) Twelve-sided Barrel ECAL only. (4) Two hexagonal end cap ECAL only. (5) 3D mesh of the pressure vessel produced by the Gmsh software. (6) Image of the dual-anode TPC produced by ElmerGUI. Red Circular ring is a single voltage strip.

In the first image above, the interior hexagon outlines the end cap ECAL. The surrounding concentric circles (annulus) are an outline of the insulation layer. The twelve-sided barrel ECAL surrounds, and closely hugs, the outside of the insulation layer. The outer circle marks the edge of the pressure vessel, which is commensurate with the radial boundary of the simulation.

Appendix B. Dual-Anode Design

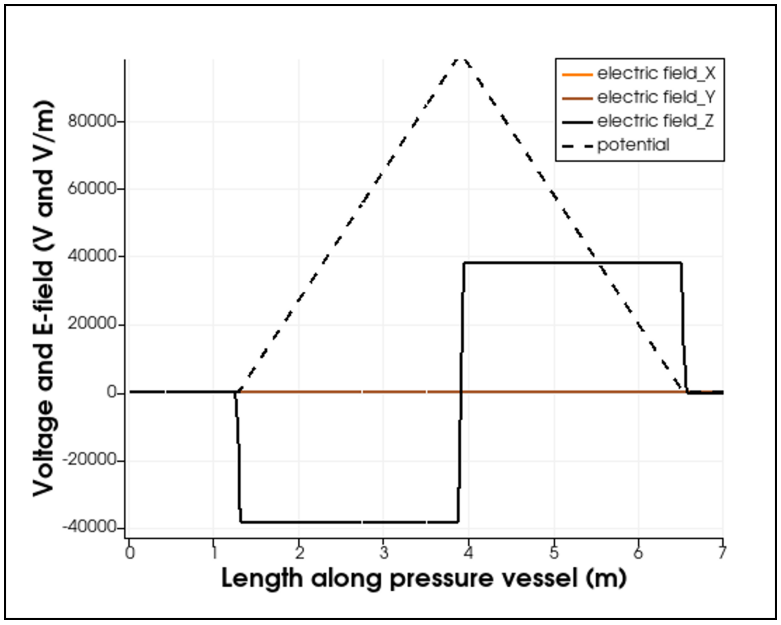

Figure A2. Voltage and field E_z on the axis of the TPC.

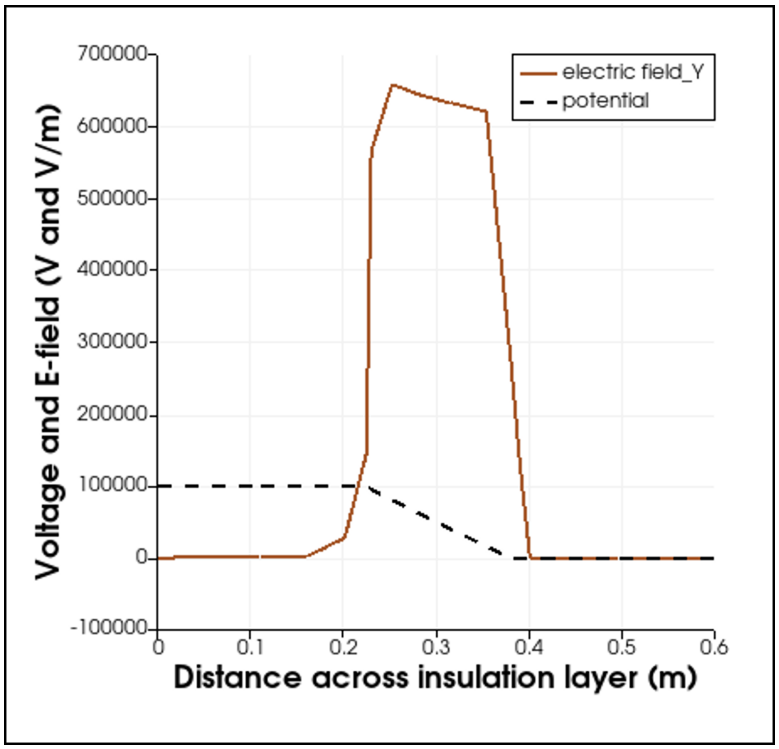

Figure A3. Voltage and fields across the insulation gap.

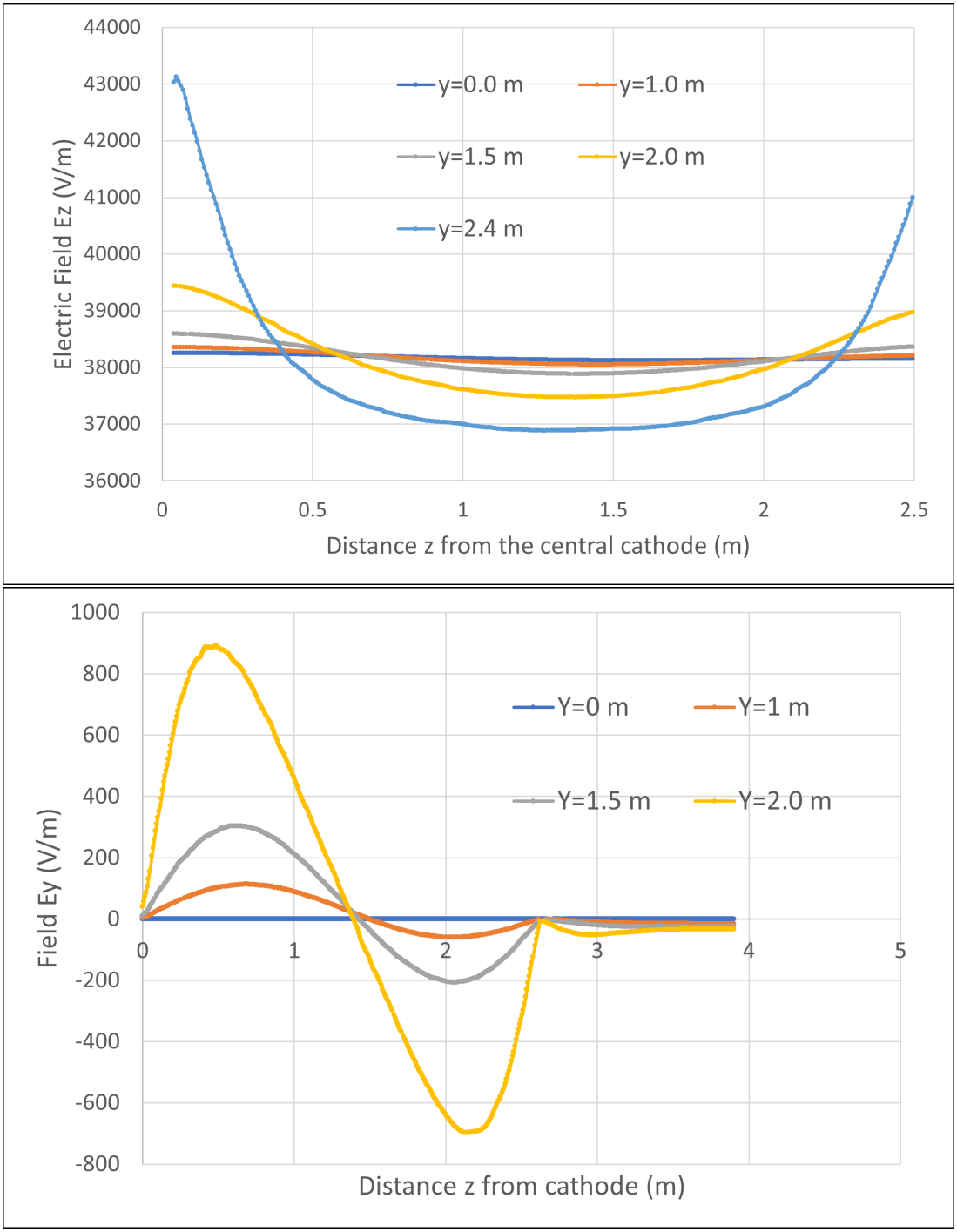

Figure A4. Electric field component E_z for the dual-anode design.

Appendix C. Single-Anode Design

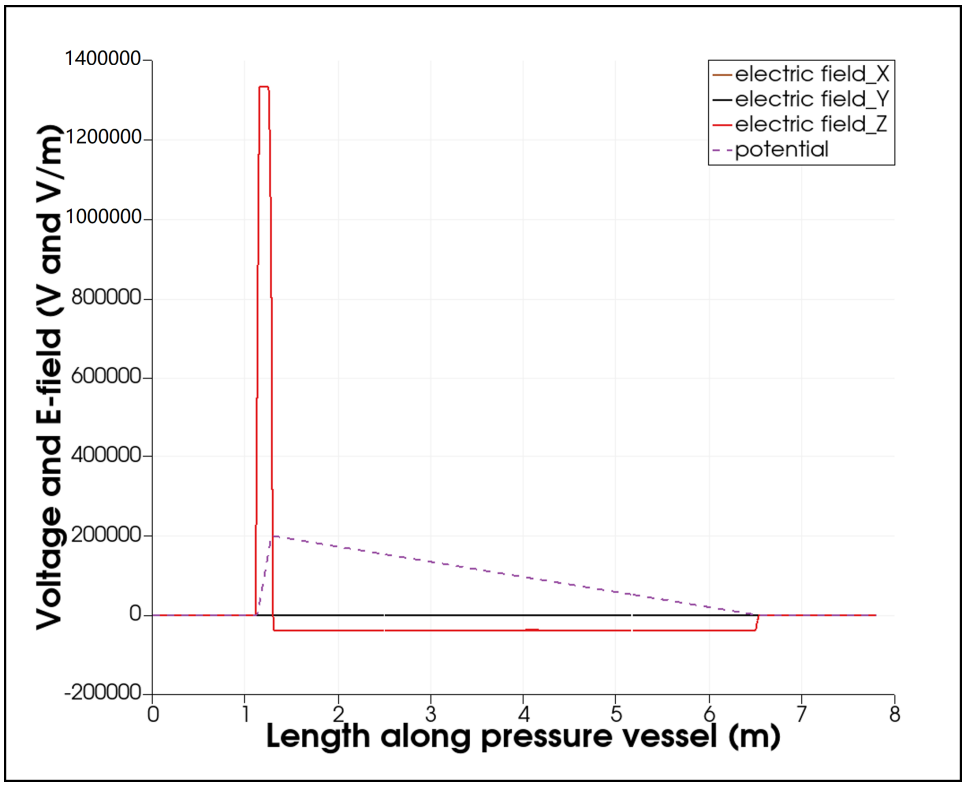

Figure A5. Plot of voltage and fields through the central axis of the TPC for the single-anode design.

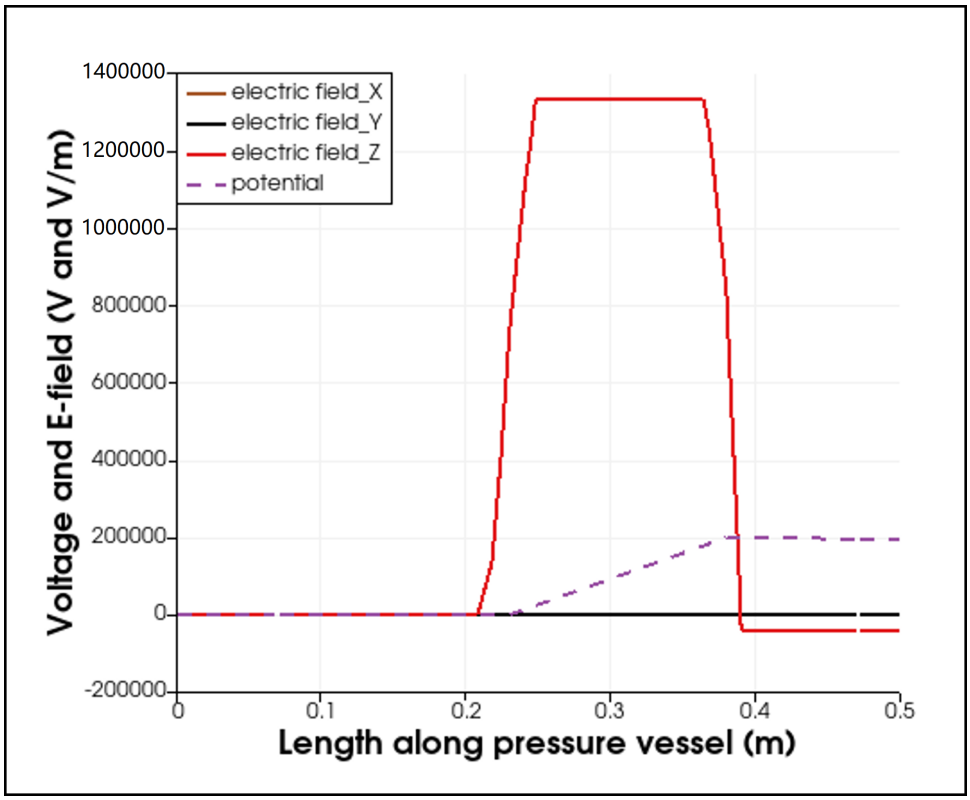

Figure A6. Voltage and fields across the insulation gap.

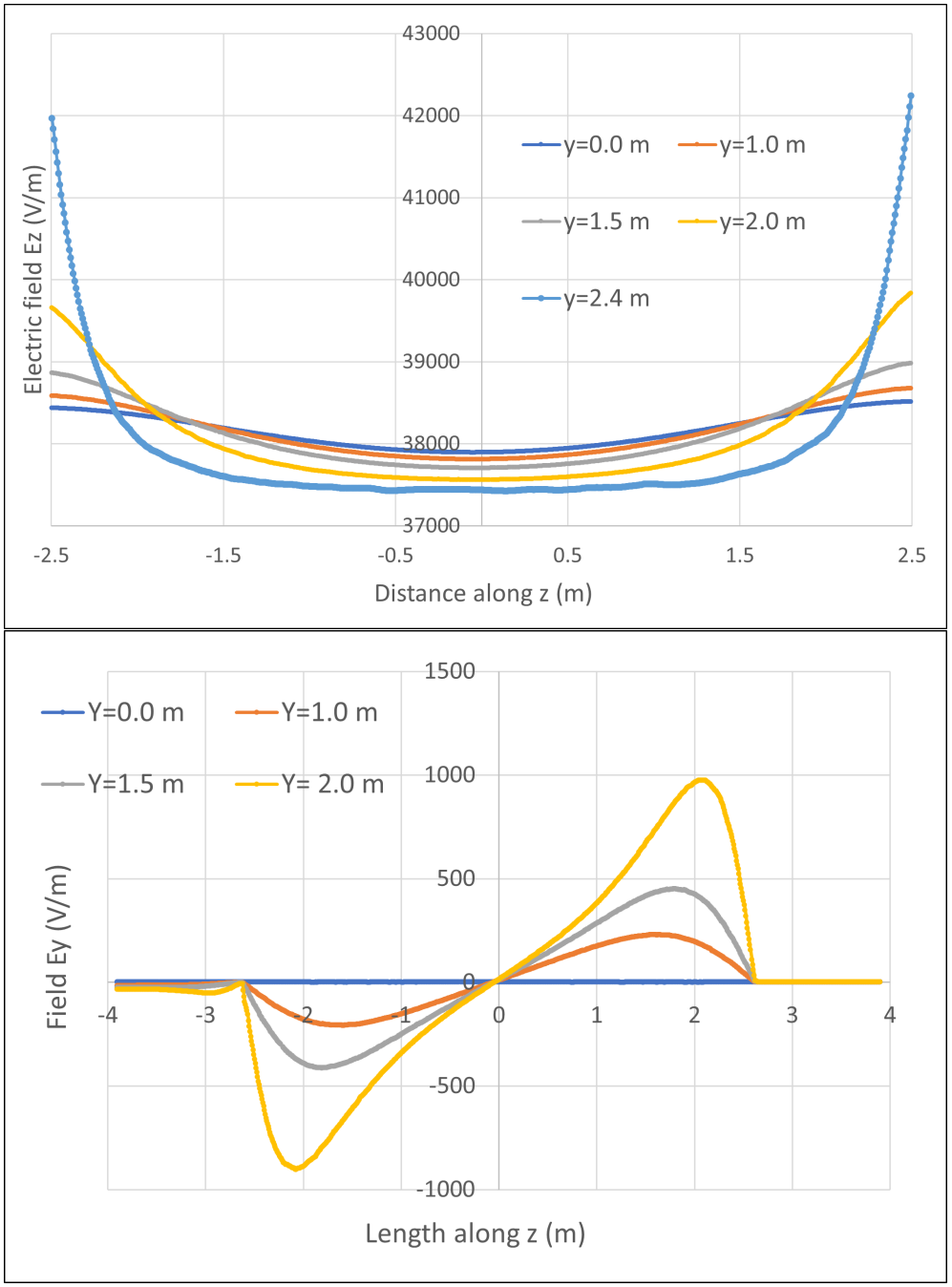

Figure A7. (**Top**): Electric field component E_z for the single-anode design. (**Bottom**): Electric field component E_y for the single-anode design.

References

1. Abud, A.A.; Abi, B.; Acciarri, R.; Acero, M.A.; Adamov, G.; Adams, D.; Adinolfi, M.; Aduszkiewicz, A.; Ahmad, Z.; Ahmed, J.; et al. Deep Underground Neutrino Experiment (DUNE) Near Detector. Conceptual Design Report. *Instruments* **2021**, *5*, 31. [CrossRef]
2. Abi, B.; Acciarri, R.; Acero, M.A.; Adamov, G.; Adams, D.; Adinolfi, M.; Ahmad, Z.; Ahmed, J.; Alion, T.; Alonso Monsalve, S.; et al. Deep Underground Neutrino Experiment (DUNE), Far Detector Technical Design Report, Volume I, Introduction to DUNE. Available online: https://arxiv.org/abs/2002.02967 (accessed on 13 February 2022).
3. Dellacasa, G.; Ramello, L.; Scalas, E.; Sitta, M.; Ahmad, N.; Ahmad, S.; Ahmad, T.; Bari, W.; Irfan, M.; Zafar, Z.; et al. ALICE: Technical Design Report of the Time Projection Chamber. Available online: http://cds.cern.ch/record/451098 (accessed on 13 February 2022).

4. Alme, J.; Andres, Y.; Appelshäuser, H.; Bablok, S.; Bialas, N.; Bolgen, R.; Bonnes, U.; Bramm, R.; Braun-Munzinger, P.; Campagnolo, R.; et al. The ALICE TPC, a large 3-dimensional tracking device with fast readout for ultra-high multiplicity events. *Nucl. Instrum. Meth. A* **2010**, *622*, 316–367. [CrossRef]
5. Geuzaine, C.; Remacle, J.-F. Gmsh: A Finite Element Mesh Generator with Built-In Pre- and Post-Processing Facilities. Available online: http://www.as.dlr.de/hiocfd/gmsh.pdf (accessed on 13 February 2022).
6. Raback, P. ElmerGrid Manual. Available online: http://69.63.68.22/archive/science/physics/elmer/doc/ElmerGridManual.pdf (accessed on 13 February 2022).
7. Lyly, M. Takayuki, S. ElmerGUI Manual. Available online: http://www.nic.funet.fi/index/elmer/doc/ElmerguiManual.pdf (accessed on 13 February 2022).
8. Elmer non-GUI Tutorials. Available online: http://69.63.68.22/archive/science/physics/elmer/doc/ElmerTutorials_nonGUI.pdf (accessed on 13 February 2022).
9. Ruokolainen, J.; Malinen, M.; Raback, P.; Zwinger, T.; Pursula, A.; Byckling, M. ElmerSolver Manual. Available online: http://www.nic.funet.fi/index/elmer/doc/ElmerSolverManual.pdf (accessed on 13 February 2022).
10. Ayachit, U. *The ParaView Guide*; Kitware Inc.: Clifton Park, NY, USA, 2020.
11. Moreland, K. *The ParaView Tutorial, Version 5.6*; Sandia National Laboratories: Albuquerque, NM, USA, 2018.
12. Bross, A. (Fermi National Accelerator Laboratory, Batavia, IL, USA); Bersani, A. (Istituto Nazionale di Fisica Nucleare, Sezione di Genova, Genoa, Italy). Personal communication, 2021.
13. Uhlig, H.H.; Keyes, F.G. The Dependence of the Dielectric Constants of Gases on Temperature and Density. *Chem. Phys.* **1933**, *1*, 155. [CrossRef]
14. Norman, L.; Silva, K.; Jones, B.J.P.; McDonald, A.D.; Tiscareno, M.R.; Woodruff, K. Dielectric Strength of Noble and Quenched Gases for High Pressure TPCs. *Eur. Phys. J. C* **2021**, *82*, 52. Available online: https://link.springer.com/article/10.1140/epjc/s10052-021-09894-z (accessed on: 13 February 2022). [CrossRef]